Stratified Spectral Mixture Analysis of Medium Resolution Imagery for Impervious Surface Mapping

Genyun Sun[1], Xiaolin Chen[2], Jinchang Ren[3], Aizhu Zhang[1], Xiuping Jia[2]

[1]School of Geosciences, China University of Petroleum (East China), Qingdao, Shandong 266580, China

[2] School of Electrical Engineering, The University of New South Wales at Canberra, ACT 2600, Australia

[3] Department of Electronic and Electrical Engineering, University of Strathclyde, Glasgow G11XQ, U.K.

Abstract

Linear spectral mixture analysis (LSMA) is widely employed in impervious surface estimation, especially for estimating impervious surface abundance in medium spatial resolution images. However, it suffers from a difficulty in endmember selection due to within-class spectral variability and the variation in the number and the type of endmember classes contained from pixel to pixel, which may lead to over or under estimation of impervious surface. Stratification is considered as a promising process to address the problem. This paper presents a stratified spectral mixture analysis in spectral domain (Sp_SSMA) for impervious surface mapping. It categorizes the entire data into three groups based on the Combinational Build-up Index (CBI), the intensity component in the color space and the Normalized Difference Vegetation Index (NDVI) values. A suitable endmember model is developed for each group to accommodate the spectral variation from group to group. The unmixing into the associated subset (or full set) of endmembers in each group can make the unmixing adaptive to the types of endmember classes that each pixel actually contains. Results indicate that the Sp_SSMA method achieves a better performance than full-set-endmember SMA and prior-knowledge-based spectral mixture analysis (PKSMA) in terms of R, RMSE and SE.

Key words—Impervious surface, Stratification, Spectral mixture analysis, CBI

1. Introduction

Impervious surface is defined as any area consisting of constructed surface which water cannot infiltrate to reach the soil (Yang et al, 2010; Weng, 2012), such as roads, roofs, and parking lots. It not only serves as a key indicator of the degree of urbanization, but also affects in the micro-ecosystem change (Wang et al, 2015). The increasing replacement of nature landscape by impervious surface leads to the change of hydrological character (White & Greer, 2006; Xian et al, 2007; Du et al., 2015), the generation of heat island effects (Kato & Yamaguchi, 2007; Yuan & Bauer, 2007; Coseo & Larsen, 2014), deterioration in water quality (Conway, 2007) and other detrimental effects. Therefore, it is essential to monitoring impervious surface distribution timely and accurately to ensure urban development is sustainable (Wu & Murray, 2005; Du & Du, 2014).

Remote sensing technology has become an important method, and may be the only viable way, to effectively extract impervious surface due to its high efficiency and low cost with large coverage (Yang et al, 2010; Lu & Weng, 2006). Various studies have been conducted for impervious surface mapping, with images from a large range of satellite sensors and a variety of data sources, including MODIS images with coarse spatial resolution (Yang & Lunetta, 2011; Deng & Wu, 2013), Landsat TM/ETM+ and ASTER imagery (Hu & Weng, 2009; Sexton et al, 2013) with moderate spatial resolution, and IKONOS and QuickBird data (Lu & Weng, 2009; Zhou & Wang, 2008) with high spatial resolution. In addition to the optical remote sensing data, some other types' data, such as nighttime photography (Kotarba & Aleksandrowicz, 2016), Synthetic Aperture Radar (SAR) imagery (Zhang et al, 2016; Zhang et al, 2014) and open social data (Hu et al, 2016), have also been studied on their application to impervious surface estimation in recent years. Among them, medium spatial resolution images might be a better choice for the urban impervious surface mapping, because they provide a good trade-off among coverage, price, and quality.

However, due to the heterogeneity of urban land covers and the limitation in spatial resolution, the presence of mixed pixels has been recognized as a major problem in the analysis of medium spatial resolution images (Weng, 2012). Several unmixing methods have then been applied for impervious surface extraction, including linear spectral mixture analysis (LSMA) (Weng et al, 2009; Hu & Weng, 2008; Yang & He, 2017), artificial neural network (ANN) (Mohapatra and Wu, 2008), regression analysis (Yang et al, 2003; Yang & Liu, 2005; Kaspersen et al., 2015) and regression trees (Huang & Townshend, 2003; Deng & Wu, 2013). Yet LSMA is still the most popular approach due to its simplicity and physically-based description of the fractions of different land covers (Small & Milesi, 2013; Burazerovic et al, 2013).

While LSMA and LSMA based methods are easy to use in estimating impervious surface, several problems still exist. It has been found that impervious surface tends to be overestimated in the areas with small amounts of impervious surface, but is underestimated in the areas with large amounts of impervious surface (Weng, 2012; Lu and Weng, 2006). The similarity in spectral properties between impervious and pervious surface, especially impervious surface and soil, can be one of the main reasons for underestimation in urban area and overestimation in pervious area. Another problem is the difficulty in selecting endmembers due to within-class spectral variability (Foody et al, 1997). It should be noted that the differences in type, geometry and illumination etc. lead to the huge differences in term of spectral characteristics of impervious surface. Therefore, using one endmember to represent all types of impervious surfaces is often found problematic (Weng et al, 2008). The performance of LSMA can also be reduced if every pixel in the image is unmixed into a fix set of endmembers, where some pixels may only contain a subset of endmembers.

Stratification is considered as a promising process to solve these problems. In (Lu & Weng, 2004), stratification of a whole scene into subareas with similar landscape structures is suggested to improve impervious surface mapping. Several studies (Wu & Murray, 2003; Zhang et al, 2014; Small, 2001; Somers et al,2009) have attempted to employ different endmember class sets for urban and rural areas. However, the endmembers sets applied to each subarea are extracted from the entire image scene. The weakness of this treatment is the spectral variability in different subsets is not considered. The endmembers, which are selected at the extreme of an n-dimensional scatter plot of the entire image may be less representative as the pure pixels in each subset (Deng & Wu, 2013). The current methods stratify a remote sensed image into urban and rural areas through spatial information, such as texture and road density information (Zhang et al, 2014; Liu & Yang, 2013). The overlooked the spectral information would result in mis-estimation of land cover abundances.

In this study, we address the above mentioned problems and propose a stratified spectral mixture analysis in spectral domain (Sp_SSMA) for impervious surface mapping. We clipped an image data set into three groups to reduce the within class variability in each subgroup based on three spectral character components, namely Combinational Build-up Index (CBI)(Sun et al, 2015), Normalized Difference Vegetation Index (NDVI) (Rouse et al, 1974) and color intensity. Then, endmembers are selected from each group independently rather than from the entire image to cope with the within class variability. An endmember set with different types and numbers is applied in each group to make it more adaptive. Impervious surface fractions are estimated by LSMA and the results of the three subgroups are combined to produce a complete map.

The remainder of this article is structured as follows. The second section presents the methodology of Sp_SSMA, including the stratification, the selection of endmembers and the procedures for deriving impervious surface abundance. The third section introduces the study areas and remotely sensed data, including data preprocessing. The comparative results and discussions are reported in Section 4. Finally, conclusions are provided in Section 5.

2. Methodology

Based on the definition, impervious surface is a unifying theme. However it consists of a number of artificial features which have different spectral profiles in general. Figure 1(a) illustrates the mean spectral values of different impervious surface and other major land cover classes based on the pure pixels selected from a Landsat TM image. It indicates that not only impervious surfaces consist of different structures, colors, and materials, vegetation and soil also show great spectral differences within each of them. Figure 1(b) is the corresponding grouped scatter points of the sampled pixels in the feature space composed by the first two components of minimum noise fraction (MNF1and MNF2). We can see that the pure pixels are not always located at the extremes of the scatter plot as it supposed to be theoretically, due to the within-class variation of a land cover type. It also indicates the spectral variability within several classes as well as the spectral confusion among several land covers, especially between urban impervious surfaces and bare soil.

Therefore, simply extracting a single set of endmembers from the vertices in an n-dimensional scatter plot of an entire scene, like the treatment in (Powell, et al, 2007), is potentially less reliable because they cannot account for the considerable within-class variability (Rashed et al, 2003; Roessner et al, 2001). The similarity of spectral characteristics between impervious and pervious surface, especially bare soil, also prevent the SMA-based methods from achieving a promising result.

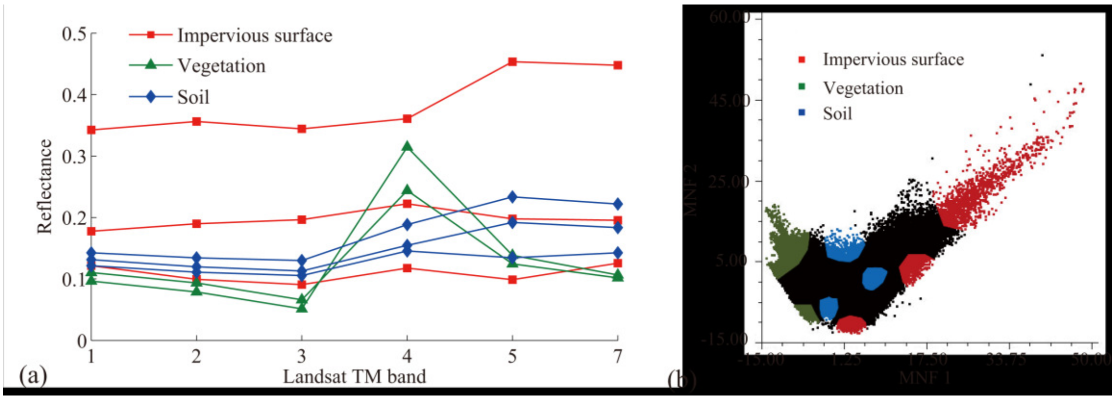

Figure 1 Reflectance of land feature endmembers (a) and the corresponding feature space representation of the first two MNF components for Landsat TM reflectance image (b).

To tackle this problem, we develop a stratified spectral unmixing method in spectral domain (Sp_SSMA). Three spectral feature components, CBI, intensity component of intensity-hue-saturation (IHS) and NDVI, are utilized to partition the entire data into three groups, named Group 1, Group 2 and Group 3. Each group is processed independently, including endmember extraction and spectral unmixing, to minimize the within class spectral variability and the confusion between some urban features and non-impervious land covers. The major steps in Sp_SSMA are described in Figure 2.

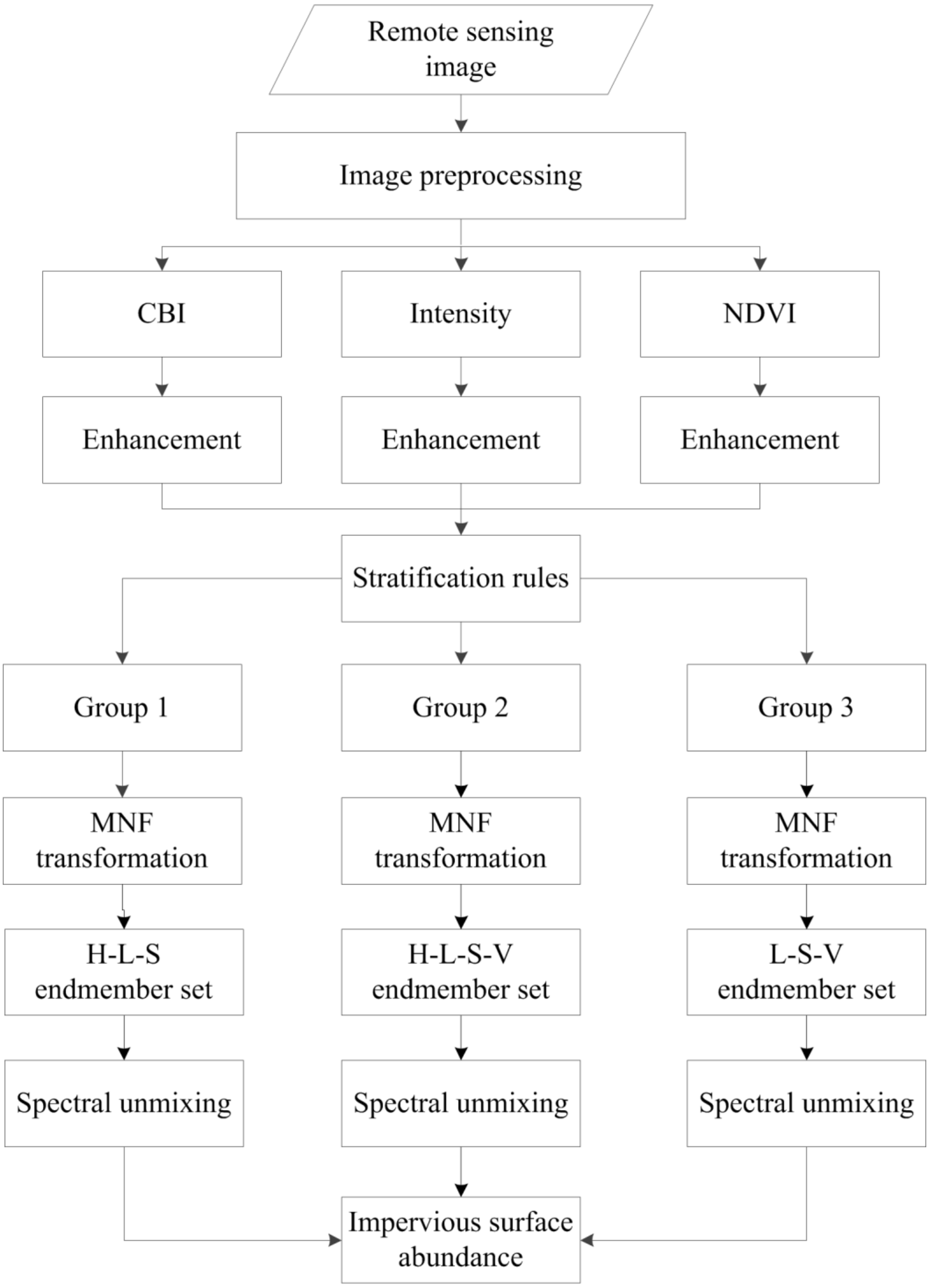

Figure 2 Flowchart of the Sp_SSMA method.

2.1 Stratification

2.1.1 CBI calculation

CBI is a feature-extraction based spectral impervious surface index. It reduces the original multi-/hyper-bands into three thematic-oriented features. They are the first component of a principal component analysis (PC1), Normalized Difference Water Index (NDWI) (Gao, 1996) and Soil Adjusted Vegetation Index (SAVI) (Huete, 1988), to represent high albedo, low albedo and vegetation respectively. The features are calculated using the following equations (Sun et al, 2015):

$$CBI=\frac{(PC1_{nor}+NDWI_{nor})/2-SAVI_{nor}}{(PC1_{nor}+NDWI_{nor})/2+SAVI_{nor}} \qquad (1)$$

with

$$SAVI=\frac{(\rho_{NIR}-\rho_{RED})(1+L)}{\rho_{NIR}-\rho_{RED}+L} \qquad (2)$$

$$NDWI=\frac{\rho_{GREEN}-\rho_{NIR}}{\rho_{GREEN}+\rho_{NIR}} \qquad (3)$$

where $\rho_{GREEN}, \rho_{RED}, \rho_{NIR}$ represent the reflectance value of GREEN, NIR and SWIR bands, respectively. L is a correction factor ranging from 0 to 1. In this study, 0.5 is taken to form a vegetation image. $PC1_{nor}, SAVI_{nor}$ and $NDWI_{nor}$ are the normalized PC1, SAVI and NDWI respectively.

In CBI, impervious surfaces are highlighted with positive values, vegetation is represented with negative values while bare soil and mixed land cover types are associated with numerical values about zero. Qualitative and quantitative assessments of accuracy analysis, separability between impervious surface and soil at different spatial and spectral resolutions as well as comparison with other indices indicate that CBI is a promising and reliable urban landscape index for mapping impervious surface areas (Sun et al, 2015).

2.1.2 I calculation

The IHS color space can be regarded as a two-dimensional color vector and one intensity vector (Córdoba-Matson et al, 2010). That is to say, the spectral magnitude of a land feature mainly lies in the intensity component, which is expressed as

$$I=\sum_{i=1}^{n}\rho_{VIR-i}/n \qquad (4)$$

where ρ_{VIR-i} is the ith VIR band of a pixel, n is the total number of VIR bands. The intensity value of the bright impervious surface tends to show the largest distinction with the background land features.

2.1.3 NDVI calculation

NDVI (Rouse et al, 1974) is an effective index to measure vegetation content which employs the peak and valley reflectances at NIR and RED bands to form the vegetation index (Huete, 1988). In this study, NDVI is utilized to make the distinction of vegetation due to their high NDVI values. The NDVI is calculated using Eq. (5)

(Rouse et al, 1974).

$$NDVI=\frac{\rho_{NIR}-\rho_{RED}}{\rho_{NIR}+\rho_{RED}} \qquad (5)$$

where ρ_{RED} and ρ_{NIR} represent the reflectance values of GREEN, NIR and SWIR bands, respectively.

2.1.4 Threshold selection

The threshold selection for stratification is crucial to delineate the biophysical distribution of the impervious surface from other land covers. In this study, a transformation (Liu et al, 2011) was utilized to improve the separability between different land cover types. The gray-scaled index images, namely CBI, I and NDVI, were enhanced by adopting Eq. (6) (Liu et al, 2011).

$$i_{enh}=(\frac{1}{\pi}\arctan[\lambda\pi(i_{nor}-\theta)]+0.5)\sqrt{i_{nor}} \qquad (6)$$

Where i_{enh} is the enhanced index map, i_{nor} is the normalized index map, λ is a sensitivity factor and θ is the coarse estimation of mean value of the target land cover type, or more precisely impervious surface in CBI and I while vegetation in NDVI.

The enhanced intensity maps are used to stratify the whole image. Otsu (Otsu, 1979) proposed a histogram-based threshold selection method that is suitable for separating an object from its background. We use this method to automatically select the threshold T for stratification. In Otsu's method (Otsu, 1979), a threshold T is selected to maximize

$$6^2(T)=\frac{(\mu\omega_1(T)-\omega_2(T))^2}{\omega_1(T)\omega_2(T)} \qquad (7)$$

where $\omega_1(T)=\sum_{i=0}^{T}p_i$, $\omega_2(T)=\sum_{i=T+i}^{255}p_i$,$\mu=\sum_{i=0}^{255}ip_i$, and p_i is the probability of the gray level i. T_{CBI}, T_I and T_{NDVI}, the threshold of the enhanced CBI, I and NDVI respectively, are obtained using Eq. (7) and used to stratify the image. Three groups are defined as follows.

Group 1: $CBI_{enh}>T_{CBI}$, $I_{enh}>T_I$ and $NDVI_{enh}<T_{NDVI}$

Group 3: $CBI_{enh}<T_{CBI}$ and $NDVI_{enh}>T_{NDVI}$

Group 2: $\left((CBI_{enh}<T_{CBI})\cap(NDVI_{enh}<T_{NDVI})\right)\cup\left((CBI_{enh}>T_{CBI})\cap(I_{enh}<T_I)\right)\cup((CBI_{enh}>T_{CBI})\cap(I_{enh}>T_I)\cap(NDVI_{enh}>T_{NDVI}))$, (i.e. is the remaining region.)

2.2 Endmember selection

Endmember extraction is critical. In this study, endmembers were selected in each group independently, rather than from the entire image, to achieve more adaptive spectral characters. The endmember selection in each subset follows the usual minimum noise fraction (MNF)-based procedure. Spectral feature spaces were generated using the first three MNF components, and the typical pure pixels are those located at the extreme vertices of the data cloud in the scatter plots. Endmembers of the three sub-regions were indentified from the vertices of the scatterplots in each sub-scene independently. The extreme or less extreme pure pixels in the original image located at the extreme points in different groups so as to balance the within class variation and easy implement of extreme pixels selection. The number and type of endmember sets in each sub-region is determined based on the corresponding respective biophysical characteristics.

The combined criteria of Group 1 can make it reasonable to treat Group 1 data as containing no vegetation component. That is to say, Group 1 is composed of impervious surface and soil with vegetation pixels masked out by intensity component and NDVI. In contrast, the area of Group 3, which contains a low CBI value and high NDVI value, is mainly composed of vegetation and soil, with small amount of low albedo impervious surface. As for Group 2, impervious surface (high albedo and low albedo), soil and vegetation form the land cover features. Therefore, different endmembers are defined for each Group as follows.

Group 1: high-albedo, low albedo and soil (H-L-S).

Group 2: high albedo, low albedo, soil and vegetation (H-L-S-V).

Group 3: low-albedo, soil and vegetation (L-S-V).

2.3 Impervious surface estimation

The LSMA approach is physically based on the assumption that the spectrum for each pixel is a linear combination of all endmembers in the pixel (Wu, 2004) with the proportions of the endmembers representing the percentage of the land feature. The fraction image of each endmember is estimated through inversion of the linear combination with the spectral proportions of the endmembers representing the percentage of the land feature. LSMA was also under the assumption that no interaction between the photons reflected by each component. With these assumptions, a LSMA with full abundance constraints can be expressed as (Lu & Weng, 2006):

$$R_b = \sum_{i=1}^{N} f_i R_{i,b} + e_b \qquad (8)$$

where

$$\sum_{i=1}^{N} f_i = 1 \wedge f_i \geq 0 \qquad (9)$$

where R_b is a mixed pixel's reflectance at band b, N is the number of endmembers, $R_{i,b}$ is the reflectance of endmember i at band b, f_i is the fraction of endmember i, and e_b is the residual error.

As high and low albedo endmembers both are associated to impervious surface, the final impervious surface fraction is calculated by summing the abundance of high and low albedo endmembers for each mixed pixel. Then, the impervious surface abundance in the three urban subsets was mosaicked to build the final regional impervious surface abundance map.

3 Study area and data

Multi-sensor data, namely Landsat TM and ASTER, with two study sites were investigated to test he proposed Sp_SSMA algorithm (Figure 3).

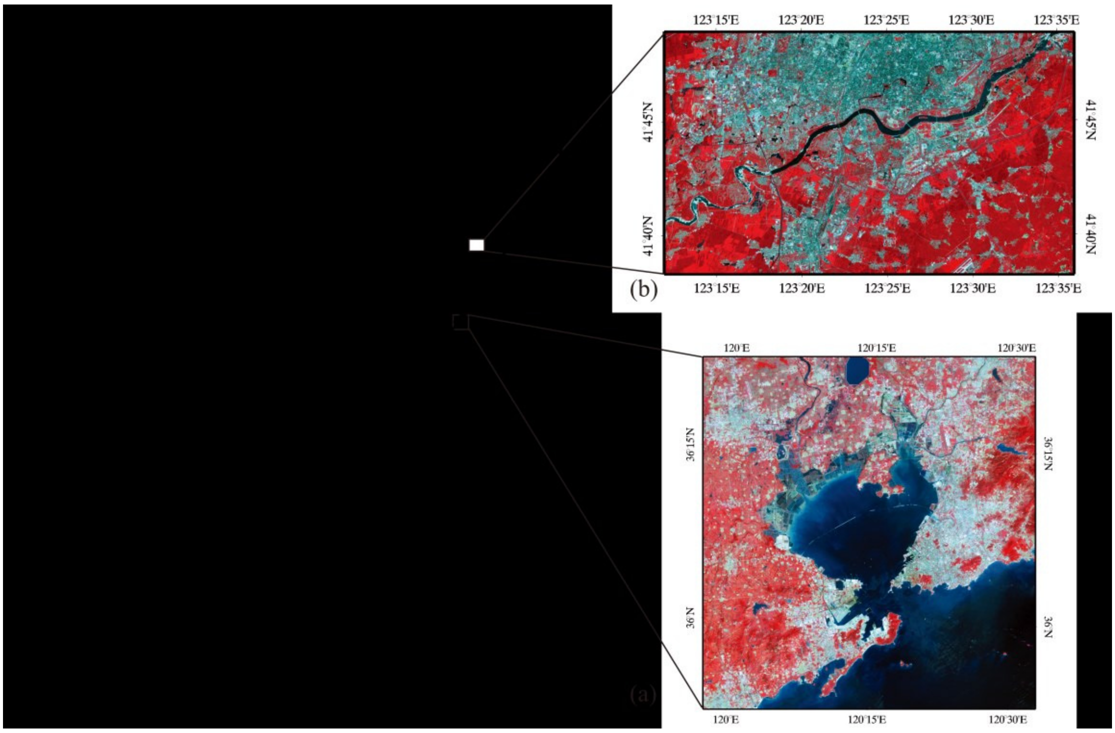

Figure 3 The location of study area: (a)The false color image covering the Qingdao city, China, illustrated with Landsat TM image (R: band 4, G: band 3, B: band 2), (b)The false color image covering the Shenyang city, China, illustrated with ASTER image (R: band 3, G: band 2, B: band 1).

3.1 Landsat TM imagery

The first study area is an urban transect in the region of Qingdao, China. As shown in Figure 3(a), a scene of Landsat TM image acquired on July 15, 2009 was employed for this study, suggesting that a large diversity of land cover properties present within the study area. Different impervious surfaces, such as residential areas, mixed-use areas, commercial and industrial districts, are shown in the image. Non-urban land cover types include water bodies, green vegetation and bare soils.

The city of Qingdao is situated in the south of the Shandong Province, adjacent to the Huanghai Sea (Figure 3(a)). As an important region in Eastern China, Qingdao has seen rapid development. The annual GDP reached 869.2 billion Yuan in 2014, with an increase of 8.0%, ranking first in Shandong Province and fourteenth out of China's top 20 cities. The fast economic growth is accompanied by rapid urbanization, causing transformation from nature environment to man-made surface. As for urban area, the historic town is located in the eastern part of the study area while the new district mainly lies in the western part. The suburban area is dominated by forest land while agriculture land located mainly in the northern part of the study area.

3.2 ASTER imagery

The second study area (Figure 3(b)), located in Shenyang, China, is a typical heavy industrial area since early 1900s. Aster imagery was collected over the area on August 17, 2004. Shenyang is the provincial capital and largest city of Liaoning Province, as well as an important heavy industrial base and a transportation hub in Northeast China. Under the reform and open policies, Shenyang has experienced sustained and high speed growth and urbanization since the late 1970s. After the "revitalizing the old industrial bases in Northeastern China" strategy in 2003, Shenyang was identified as the core of the new-industrialization zone for national demonstration (Zhang et al, 2007). It is expected to offer a demonstration for China's change in industrial and economic development mode. Under such circumstances, Shenyang's urbanization will definitely continue to increase rapidly, and a more complex landscape resulting from industrial transformation will be observed.

3.3 Data preprocessing

The Landsat TM image has six spectral bands (except the thermal band) with a spatial resolution of 30m. The ASTER image has 9 bands with different spatial resolutions (except the thermal bands), two visible bands, and one near infrared (NIR) band with the spatial resolution of 15 m, six short wavelength IR (SWIR) bands with 30m resolution. The 15m ASTER bands were resampled to 30m with the application of nearest-neighbor resampling algorithm.

Atmospheric correction was applied to neither of the images due to generally good weather condition. Radiation calibration was conducted prior to data processing. With the Landsat TM and ASTER reflectance images, water pixels were identified and removed with the help of unsupervised classification. Additionally, the Google Earth images acquired on July 22, 2009 and Oct 19, 2004 were used as ground reference data for accuracy assessment respectively.

4 Experimental Results and Discussions

4.1 Experimental design

To evaluate the performance of the proposed method for mapping impervious surface abundance and distribution, the corresponding Google Earth images, which were generated near the acquisition date of Landsat TM and ASTER images respectively, were used as the ground reference. The spatial resolution of Google Earth images in both study areas is 0.5 m and each pixel is then treated as pure pixel.

After obtaining the estimation for the actual imperviousness and estimated imperviousness, three quantitative estimators were adopted to assess the accuracy of impervious surface abundance modeled by Sp_SSMA. They are correlation coefficient (R), root mean square error (RMSE) and systematic error (SE). Specifically, R means the statistical relationships between the estimated and actual imperviousness, RMSE reflects the relative estimated errors of impervious surface abundances, and SE measures the bias, an overall tendency of over- or under-estimation. These three accuracy metrics can be calculated using Eqs. (11) to (13) respectively as follows.

$$R = \frac{\sum_{i=1}^{N}(f_i - \bar{f})(\hat{f}_i - \bar{\hat{f}})}{\sqrt{\sum_{i=1}^{N}(f_i - \bar{f})^2 \cdot \sum_{i=1}^{N}(\hat{f}_i - \bar{\hat{f}})^2}} \tag{11}$$

$$RMSE = \sqrt{\frac{1}{N}\sum_{i=1}^{N}(\hat{f}_i - f_i)^2} \tag{12}$$

$$SE = \frac{1}{N}\sum_{i=1}^{N}(\hat{f}_i - f_i) \tag{13}$$

where $\hat{f}_i$ is the estimated impervious surface fraction of sample *i* using Sp_SSMA, $\bar{\hat{f}}$ is the mean value of the samples; f_i is the true impervious surface proportion derived from Google Earth of pixel *i*; and N is the number of samples.

In order to compare the performance of impervious surface estimation of Sp_SSMA, comparative analysis is performed with a simple fixed four-endmembers SMA (fixed SMA) and the state-of-the-art hierarchical SMA, Prior-knowledge-based spectral mixture analysis (PKSMA) (Zhang et al, 2014). As for fixed SMA and PKSMA, high albedo, low albedo, soil and vegetation are chosen as a fixed set of endmembers. The extreme pixel clusters at MNF-based feature space are utilized to identify the spectral of each endmember.

4.2 Stratification result

As presented in Section 3, the enhanced CBI, I component and NDVI values were taken to construct the subgroups for spectral unmixing. In this study, $\lambda_{CBI}, \lambda_I, \lambda_{NDVI}$ are 20 and $\theta_{CBI}, \theta_I, \theta_{NDVI}$ are 0.5 for the normalized indices in both the images. Figures 4 and 5 show the original indices images and their histograms, together with the corresponding transformed result the two study areas respectively. It is clear that the separation between impervious surface and background information in CBI, I and vegetation and background fraction in NDVI is improved effectively. The histograms clearly show the apparent separations between the lower and higher values. It is suggested that the transformation plays an active role in urban image description, which may have a positive impact on stratification.

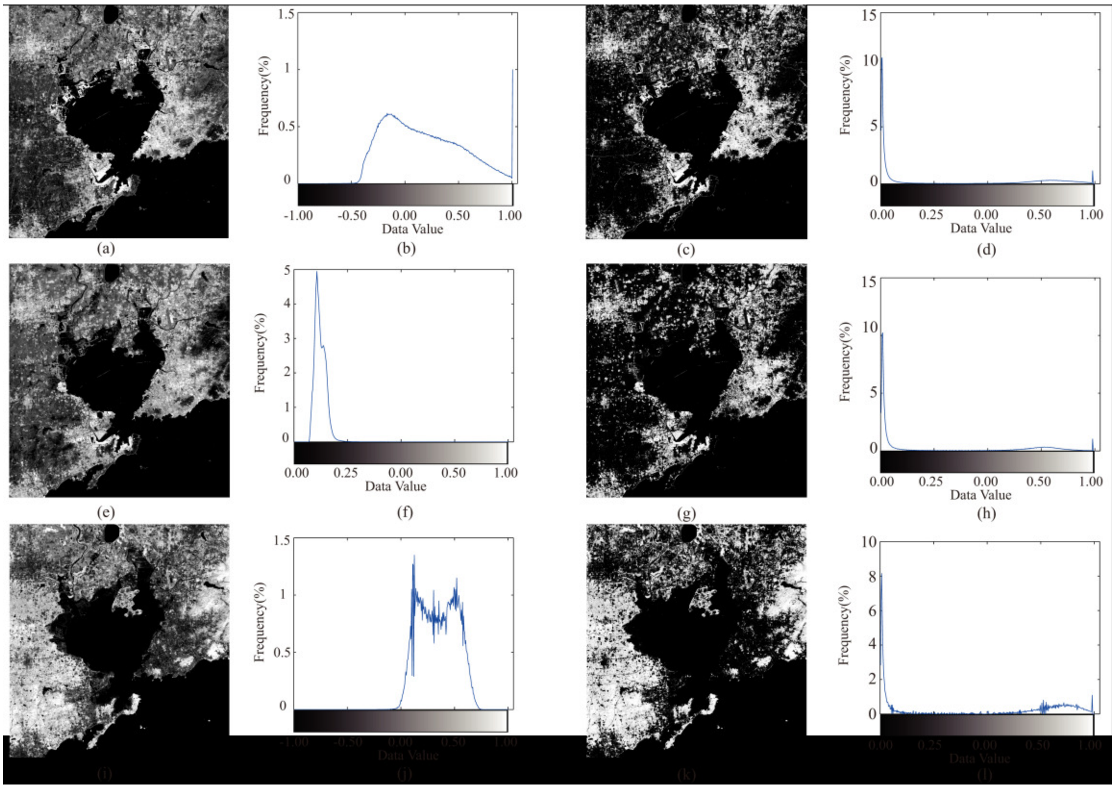

Figure 4 The transformation for feature indices enhancement in Landsat TM: (a), (e), (i) are the original CBI, I and NDVI images, (b), (f), (j) are their corresponding histogram images; (c), (g), (k) are the enhanced CBI, I and NDVI images, (d), (h), (l) are their corresponding histogram images.

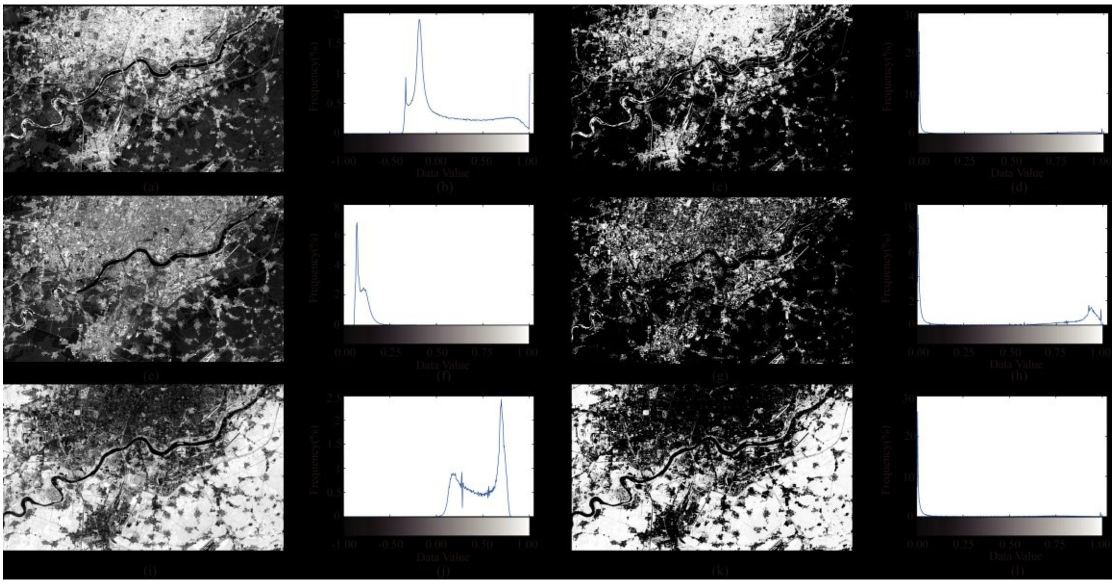

Figure 5 The transformation for feature indices enhancement in ASTER: (a), (e), (i) are the original CBI, I and NDVI images, (b), (f), (j) are their corresponding histogram images; (c), (g), (k) are the enhanced CBI, I and NDVI images, (d), (h), (l) are their corresponding histogram images.

Table 1. The threshold values.

	Landsat TM	ASTER
CBI_{enh}	0.40	0.42
I_{enh}	0.38	0.38
$NDVI_{enh}$	0.42	0.45

The automatically selected thresholds and rules for stratification in this experiment were shown in Table 1. The location of each sub-region obtained by the stratification rules (Figure 6) illustrates that Group 1 mainly lies in the new distinct in urban area, while Group 2 mainly lies in the urban fringe, industrial district and historic town, and Group 3 in suburban area. Further analysis demonstrated that the three main land cover types show significant differences among three groups. As for impervious surface, in the area of Group 1, the high and low albedo both present a relatively higher reflectance comparing with impervious surface fractions in other subsets. As for Group 2, the impervious surfaces are mainly made up of tile-roofed historic buildings, industrial area and mixed types of impervious material. The low albedo impervious surface pixels belong to Group 3 are mainly composed of metal sheet masonry. When considering the soil fraction, it tends to be composed of nature impervious land covers, such as sand and stone in construction sites and bare rocks in Group 1 and artificial land feature such as farmland and wasteland in Group 2. The nature dark bare soil is predominant in soil fractions in Group 3. Vegetation only appears in Group 2 and 3. Crops in growing season, nature grasslands, shrub lands and forest are the main composition in Group 3, whilst some artificial green land in urban area and urban fringe are graded into Group 2. As results, the three unmixing models are suitable to be applied to the three groups respectively.

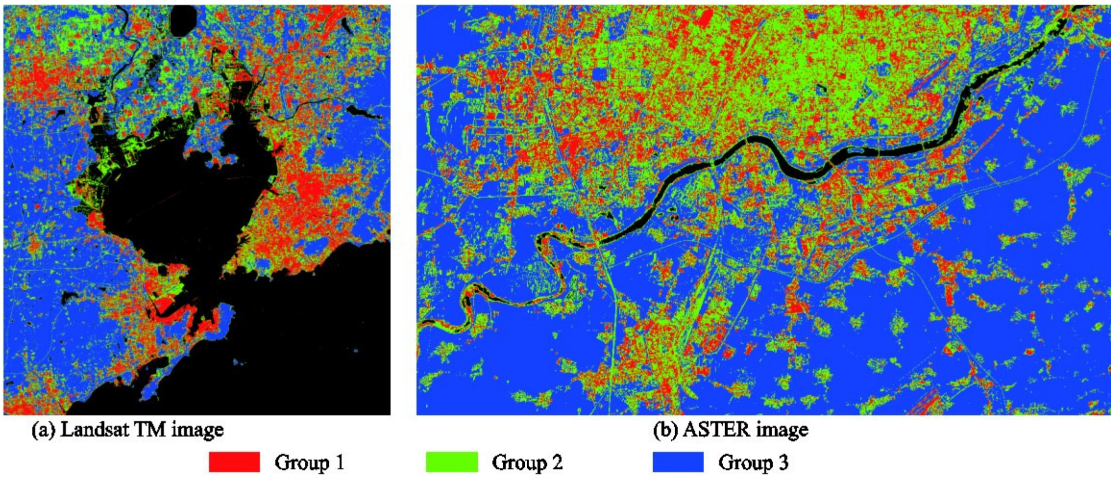

Figure 6 The stratification result: (a)Landsat TM image, (b)ASTER image.

In order to evaluate the accuracy of stratification, that is to say, there should be no vegetation fractions in Group 1 and no high albedo fractions in Group 3, 200 pixels were randomly selected in Group 1 and 3 in both study sites respectively. The overall accuracy of the stratification method were 92.75% in Group 1 and 95.50% in Group 3 with the help of Google Earth images as the reference data. The mis-stratifications were part of the error sources. Therefore, the high accuracy obtained indicates that this error can be neglected.

4.3 Impervious surface abundance

With the identified three urban area subgroups and different endmember sets achieved independently in each subarea, spectral unmixing was performed. The impervious surface abundance images are reported in Figures 7(a) and 8(a). Visual inspection found that the spatial distribution of impervious surface fraction matches well with known impervious surface distribution of Qingdao and Shenyang. A detailed insight into the general pattern of impervious surface fraction saw that the abundance value was higher in the central business district (CBD) areas and along the transportation lines, lower in suburban areas, and near zero in the rural and vegetated areas as expected. However, in less developed areas, especially the areas of Group 3, several paths of impervious surface areas failed to be recoginized which could be a primary error source.

Quantitative validations were also conducted. 400 sites were randomly selected on the Landsat and ASTER images, respectively, for validation. Each site is a window of 3 pixels by 3 pixels, covering 90 m by 90 m, since their spatial resolution is 30 m. 180 pixels by 180 pixels on the Google Earth images are associated with each site, since its spatial resolution is 0.5 m. The estimated total impervious surface abundance for each site is compared with the ground reference provided by the Google Earth images. The reason to utilize a window area to validate the performance is to reduce the problem caused by image registration error.

Quantitative analysis in Table 2 indicates that strong positive correlations with reference impervious surface fraction with relatively small RMSE and SE values with an R of 0.89 and 0.83, SE of 2.37% and 3.59%, whilst RMSE of 10.24% and 12.57% respectively. With a detailed analysis, we see a better performance is achieved in developed areas (e.g. an R of 0.86 and 0.81, an SE of 0.91% and 1.58%, a RMSE of 8.53% and 11.91%) when compared to less developed areas (e.g. an R of 0.84 and 0.79, an SE of 5.23% and 4.86%, RMSE of 12.89% and 15.32%).

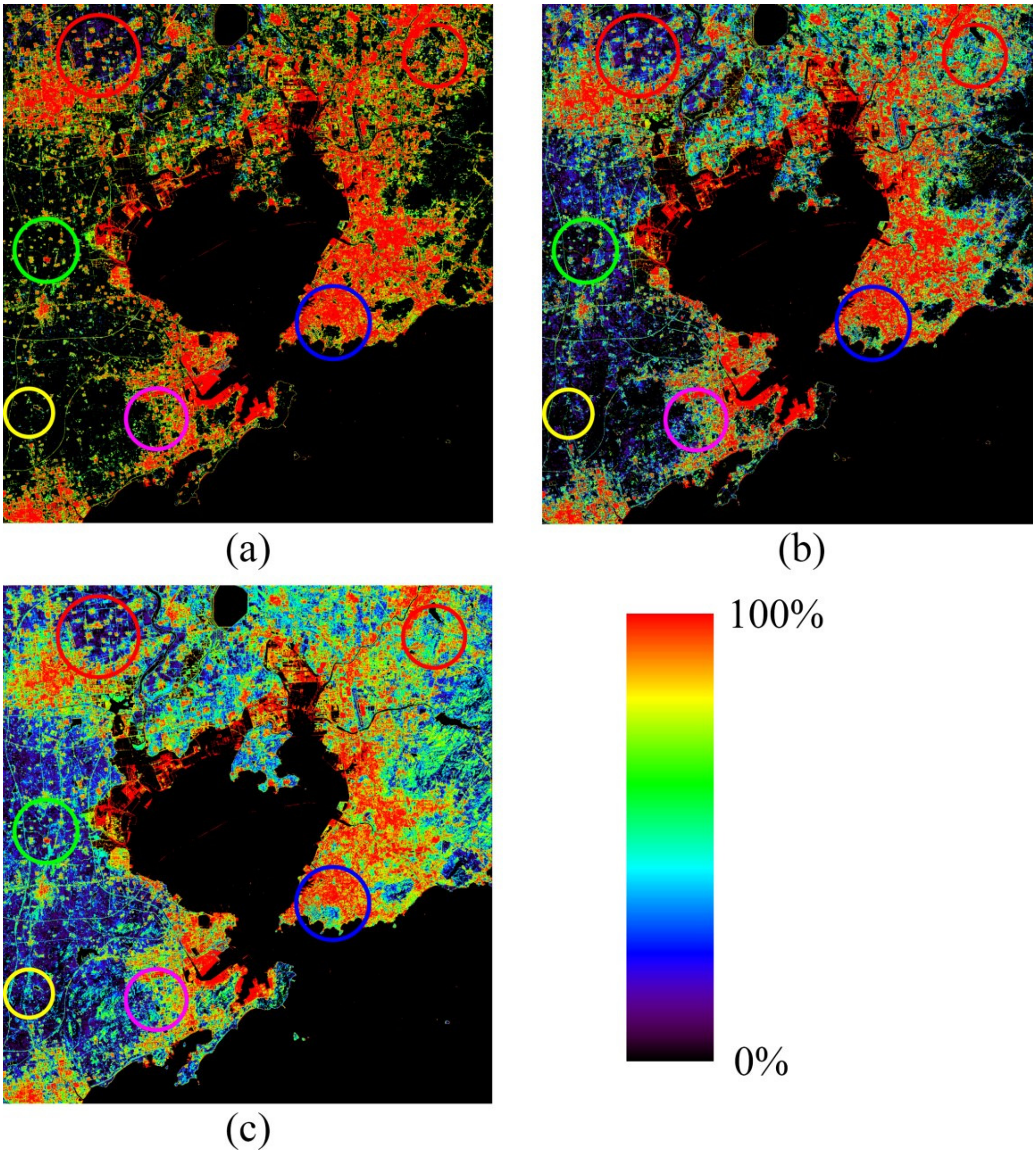

Figure 7 The impervious surface abundance images of Landsat TM using Sp_SSMA (a), PKSMA (b) and fixed-SMA(c).

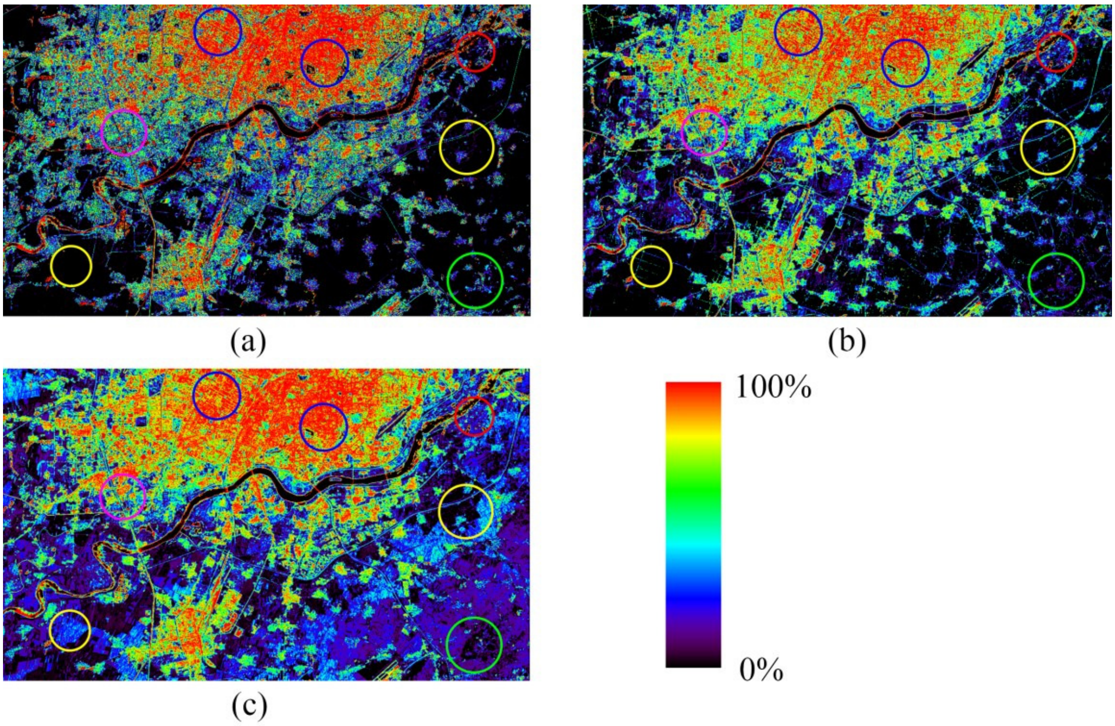

Figure 8 The impervious surface abundance images of ASTER using Sp_SSMA (a), PKSMA (b) and fixed-SMA(c).

Table 2. Accuracy assessment of impervious surfaces with Sp_SSMA, PKSMA and fixed- SMA.

		Sp_SSMA		PKSMA		Fixed-SMA	
		Landsat	ASTER	Landsat	ASTER	Landsat	ASTER
Over all	R	0.89	0.83	0.84	0.76	0.79	0.75
	RMSE	10.24%	12.57%	11.24%	17.10%	15.13%	19.28%
	SE	2.37%	3.59%	3.47%	6.11%	5.09%	8.19%
Developed	R	0.86	0.81	0.89	0.63	0.73	0.63
	RMSE	8.53%	11.91%	9.72%	14.91%	15.52%	13.02%
	SE	0.91%	1.58%	1.43%	-3.91%	-8.18%	3.34%
Less-developed	R	0.84	0.79	0.76	0.64	0.81	0.51
	RMSE	12.89%	15.32%	14.76%	19.49%	14.13%	21.22%
	SE	5.23%	4.86%	8.05%	8.47%	7.84%	12.47%

4.4 Comparative analysis

To demonstrate the effectiveness of proposed Sp_SSMA, PKSMA (Figures 7(b) and 8(b)) and fixed-SMA (Figures 7(c) and 8(c)) were carried out for comparison. Through a visual qualitative comparison, a similar impervious surface distribution illustration is observed in most parts of the study sites. Impervious surface of high abundance lies along the coastline and the northwest portion with low fraction in suburban and rural areas in Qingdao. The ASTER image, which covers an urban transect in the region of Shenyang, possesses a higher impervious surface fraction values in the north part of the study area.

However, severe misestimation can be observed in both four-endmember SMA and PKSMA. Generally, an overestimation can be observed in suburban and rural areas while the impervious surface abundance value of inner-city regions is more likely to be under-estimated in fix-SMA and PKSMA. The area in magenta circle is impervious surface mixed up with pervious materials. An obvious overestimation is observed in PKSMA in Figures 7(b) and 8(b). The land surface in red circles on Figures 7 and 8 , which are graded in Group 2 in Sp_SSMA, are ought to be mainly composed of farmland and other pervious surface which have extremely low impervious surface fraction values. Severe over-estimation can be observed in both PKSMA and four-endmember SMA. As for the area with high impervious surface fraction values, PKSMA and four-endmember SMA tend to be underestimated. On one hand, the small impervious surface patches in green circles in suburban and rural areas which are supposed to have high impervious surface abundance, are undervalued seriously in four-endmember SMA and PKSMA. On the other hand, PKSMA and fixed-SMA tend to underestimate the impervious surface fraction values in the highly urbanized old districts as marked by blue circles. This phenomenon is much more obvious in Shenyang city as reported in Figure 8. The reason lies in the inability of entire-image-achieved endmember spectrum in expressing the complex impervious surface constitution, especially in the historic towns. Shenyang, in particular, is composited of diverse industrial, commercial and residential landscape that can be traced from decades ago to present day. The industrial and economic development transformation also contributed to the complexity of impervious surface types. The results indicate that it is important that the endmembers subsets are extracted and applied in each group of data separately and highlight the advantage of spectral domain stratification. However, Sp_SSMA shows a relative poor performance in mapping transportation lines when compared with four-endmember SMA and PKSMA as shown by the region in yellow circle. The reason lies in that transportation lines are likely to be mixed up with pervious surface in suburban or rural areas due to the limited resolution. The absence of the representative endmembers leads to the poor performance on transportation lines.

The quantitative results of accuracy assessment via R, RMSE and SE are reported in Table 2. Note that these accuracy assessments were calculated for the entire image, and for developed areas (impervious surface abundance great than or equal to 30%) and less-developed areas (impervious surface abundance less than 30%)

as well. The quantitative accuracy assessment in Table 2 shows that the overall performance of the Sp_SSMA is better than the others, with R of 0.79 and 0.75, SE of 5.09 % and 8.19%, RMSE of 15.13% and 19.28% for simple four-endmember SMA, while R of 0.84 and 0.76, SE of 3.47 % and 6.11%, RMSE of 11.24% and 17.10% for PKSMA. As for the fixed-endmember SMA, a much higher error level was observed. Further analyses reveal that a severe over-estimation is given by PKSMA and four-endmember SMA in less developed areas with significantly high values of SE, and RMSE. That's because in PKSMA, some low-density areas were misclassified as high-density areas, resulting some soil were regarded as impervious surface during spectral unmixing processes on one hand. Moreover, in order to ensure the integrity of impervious surface information, NDVI and RED band doesn't always perform well in eliminate vegetation information. On the other hand, the endmember sets for all subsets in PKSMA were chosen through the original image while different combinations were applied for each subgroup. It ignored the variability within each land feature class which would lead to confusion between land cover with similar spectral characteristics. For developed areas, the performance of the PKSMA and the proposed SMA method is satisfactory and comparable in new-districts-dominated Qingdao, with old-districts-dominated Shenyang on the opposite site. When compared to Sp_SSMA, PKSMA undervalued some high abundance impervious surface in rural area with low density due to the confusion with soil. As for regions with high impervious surface fraction in urban area, overestimation can be observed due to the absence of soil endmember in high-density new district areas in PKSMA whilst old districts are suffering from underestimation. Meanwhile, PKSMA achieved a slightly better performance than that of Sp_SSMA in transportation lines.

5 Conclusions

In this paper, a stratified spectral mixture analysis in spectral domain (Sp_SSMA) method was presented for estimating the impervious surface fraction in urban areas through stratification. The Sp_SSMA takes advantage of the features of CBI, I component and NDVI to stratify the entire image into three subareas, named Group 1, Group 2 and Group 3. The performance of Sp_SSMA is demonstrated through the relationship with the impervious surfaces abundance derived from Sp_SSMA and manual digitizing which are regarded as ground reference. Moreover, visual inspection and quantitative analysis show that Sp_SSMA improved the accuracy of impervious surface estimation when compared with the existing LSMA-based method (e.g. fixed-SMA, PKSMA). A further analysis suggests that Sp_SSMA estimates impervious surface abundances in both developed and less-developed areas with satisfying results. The proposition of Sp_SSMA improved the accuracy of mapping impervious surface fraction with simple and convenient image stratification approach which may offer a help to urban land use management.

It can be considered that implementing the stratification approach into impervious surface abundance estimation may further reduce the spectral similarity between impervious surface and bare soil and reduce the within class variability in each subgroup. Though the three land cover types still suffer from intra-class variability due to the complex light scattering mechanisms in surface objects, different constituent materials, the differences between impervious surfaces are small enough to be represented by 1 or 2 endmembers while vegetation and soil can be characterized by 1 endmember respectively. Thus, Sp_SSMA can promise more reliable impervious surface fraction estimation. However, there are still confusions between impervious surface and soil in urban fringe, since the land use structures are tend to be disordered and the spectral information of impervious surface and bare soil is quite alike.

Another advantage of the proposed Sp_SSMA is that it takes advantage of stratification information to select endmembers in each sub-group independently. While stratification has been studied extensively [32], [38]-[40], little research has been conducted to consider the spectral variability in different subareas. Although the existing researches applied different endmembers to different subset, the endmembers were achieved from the entire image scene rather than each sub-area that have been classified. The Sp_SSMA takes advantage of the reduction of spectral confusion between similar objects and within class variability in each sub-group to obtain endmembers in each sub-group independently. Therefore, by using Sp_SSMA, inner layer information is made the best use.

Even though Sp_SSMA markedly improved the accuracy of impervious surface estimation, confusion between impervious surface and soil in suburban areas is still a major concern. This confusion results in the overestimation of impervious surface abundance in suburban and rural areas. More effort is still needed to address this dilemma. In addition, less estimation of the traffic roads in the rural areas is another problem to overcome. Furthermore, the accuracy and efficiency of stratification affects the result of impervious surface abundance extraction largely. Specifically, the non-existing of a specific land cover endmember, such as transformation lines in Group 2, may lead to misestimation of impervious surface fraction. Future research is needed to enhance the stratification model with more divisibility between land cover features with similar characteristics.

Acknowledgements

This work was supported by Chinese Natural Science Foundation Projects (41471353) and National Key Research and Development Program of China (Project Ref. No. 2016YFB0501501).

Reference:

Burazerovic, D., Heylen, R., Geens, B., Sterckx, S., & Scheunders, P., 2013. Detecting the adjacency effect in hyperspectral imagery with spectral unmixing techniques. IEEE Journal of Selected Topics in Applied Earth Observations & Remote Sensing, 6(3), 1070-1078.

Conway, T. M., 2007. Impervious surface as an indicator of ph and specific conductance in the urbanizing coastal zone of New Jersey, USA. Journal of Environmental Management, 85(2), 308-16.

Córdoba-Matson, M. V. Gutiérrez, J. and Porta-Gándara, M. Á., 2010. Evaluation of Isochrysis galbana (clone T-ISO) cell numbers by digital image analysis of color intensity. Journal of applied phycology, 22(4), 427-434.

Coseo, P., & Larsen, L., 2014. How factors of land use/land cover, building configuration, and adjacent heat sources and sinks explain urban heat islands in Chicago. Landscape & Urban Planning, 125(6), 117-129.

Deng, C., & Wu, C., 2013. A spatially adaptive spectral mixture analysis for mapping subpixel urban impervious surface distribution. Remote Sensing of Environment, 133(12), 62-70.

Deng, C., & Wu, C., 2013. The use of single-date modis imagery for estimating large-scale urban impervious surface fraction with spectral mixture analysis and machine learning techniques. Isprs Journal of Photogrammetry & Remote Sensing, 86(4), 100-110.

Du, Q., & Du, P., 2014. Modified multiple endmember spectral mixture analysis for mapping impervious surfaces in urban environments. Journal of Applied Remote Sensing, 8(1), 5946-5957.

Du, S., Shi, P., Rompaey, A. V., & Wen, J., 2015. Quantifying the impact of impervious surface location on flood peak discharge in urban areas. Natural Hazards, 76(3), 1457-1471.

Foody, G. M., Lucas, R. M., Curran, P. J., & Honzak, M., 1997. Non-linear mixture modelling without end-members using an artificial neural network. International Journal of Remote Sensing, 18(18), 937-953.

Gao, B. C., 1996. NDWI—a normalized difference water index for remote sensing of vegetation liquid water from space. Proc Spie, 58(3), 257-266.

Hu, T., Yang, J., Li, X., & Gong, P., 2016. Mapping urban land use by using Landsat images and open social data. Remote Sensing, 8(2), 151.

Hu, X. & Weng Q., 2008. Estimating impervious surfaces from medium spatial resolution imagery: a comparison between fuzzy classification and LSMA. Catastrophe and contention in rural China :. Cambridge University Press.

Hu, X., & Weng, Q., 2009. Estimating impervious surfaces from medium spatial resolution imagery using the self-organizing map and multi-layer perceptron neural networks. Remote Sensing of Environment, 113(10), 2089-2102.

Huang, C. & Townshend. J. R. G., 2003. A stepwise regression tree for nonlinear approximation: applications to estimating subpixel land cover.International Journal of Remote Sensing, 24(1), 75-90.

Huete, A. R., 1988. A soil-adjusted vegetation index (SAVI). Remote Sensing of Environment, 25(3), 295-309.

Kaspersen, P., Fensholt, R., & Drews, M., 2015. Using Landsat vegetation indices to estimate impervious surface fractions for European cities. Remote Sensing, 7, 8224-8249.

Kato, S., & Yamaguchi, Y., 2007. Estimation of storage heat flux in an urban area using aster data. Remote Sensing of Environment, 110(1), 1-17.

Kotarba, A. Z, Aleksandrowicz, S., 2016. Impervious surface detection with nighttime photography from the International Space Station. Remote Sensing of Environment, 176, 295-307.

Liu, J., Fang, T., & Li, D., 2011. Shadow detection in remotely sensed images based on self-adaptive feature selection. IEEE Transactions on Geoscience & Remote Sensing, 49(12), 5092-5103.

Liu, T., & Yang, X., 2013. Mapping vegetation in an urban area with stratified classification and multiple endmember spectral mixture analysis. Remote Sensing of Environment, 133(12), 251-264.

Lu, D., & Weng, Q., 2004. Spectral mixture analysis of the urban landscape in indianapolis with landsat ETM+ imagery. Photogrammetric Engineering & Remote Sensing, 70(9), 1053-1062.

Lu, D., & Weng, Q., 2006. Use of impervious surface in urban land-use classification. Remote Sensing of Environment, 102(1–2), 146-160.

Lu, D., & Weng, Q., 2009. Extraction of urban impervious surfaces from an Ikonos image. International Journal of Remote Sensing, 30(5), 1297-1311.

Mohapatra, R. P. & Wu, C., 2008. Subpixel imperviousness estimation with IKONOS imagery: an artificial neural network approach, Taylor & Francis Group: London, UK, 21-37.

Otsu, N., 1979. A threshold selection method from gray-level histograms. IEEE Transactions on Systems Man & Cybernetics, 9(1), 62-66.

Powell, R. L., Roberts, D. A., Dennison, P. E., & Hess, L. L., 2007. Sub-pixel mapping of urban land cover using multiple endmember spectral mixture analysis: manaus, brazil. Remote Sensing of Environment, 106(2), 253-267.

Rashed, T., Weeks, J. R., Roberts, D., Rogan, J., & Powell, R., 2003. Measuring the physical composition of urban morphology using multiple endmember spectral mixture models. Photogrammetric Engineering & Remote Sensing, 69(9), 1011-1020.

Roessner, S., Segl, K., Heiden, U., & Kaufmann, H., 2001. Automated differentiation of urban surfaces based on airborne hyperspectral imagery. IEEE Transactions on Geoscience & Remote Sensing, 39(7), 1525-1532.

Rouse, J. W. Haas R. H., Deering, D. W. Schell, J. A. and Harlan, J. C., 1974. Monitoring the vernal advancement and retrogradation (green wave effect) of natural vegetation. NASA/GSFC Type III Final Report, Greenbelt, MD., 371.

Sexton, J. O., Song, X. P., Huang, C., Channan, S., Baker, M. E., & Townshend, J. R., 2013. Urban growth of the Washington, D.C.–baltimore, md metropolitan region from 1984 to 2010 by annual, Landsat-based estimates of impervious cover. Remote Sensing of Environment, 129(2), 42-53.

Small, C., & Milesi, C., 2013. Multi-scale standardized spectral mixture models. Remote Sensing of Environment, 136(5), 442-454.
Small. C., 2001. Estimation of urban vegetation abundance by spectral mixture analysis. International Journal of Remote Sensing, 22(22), 299-307.
Somers, B., Delalieux, S., Verstraeten, W. W., & Verbesselt, J., 2009. Magnitude- and shape-related feature integration in hyperspectral mixture analysis to monitor weeds in citrus orchards. Geoscience & Remote Sensing IEEE Transactions on, 47(11), 3630-3642.
Sun, G., Chen, X., Jia, X., & Yao, Y., 2015. Combinational build-up index (cbi) for effective impervious surface mapping in urban areas. IEEE Journal of Selected Topics in Applied Earth Observations & Remote Sensing, 9(5), 1-12.
Wang, Z., Gang, C., Li, X., Chen, Y., & Li, J., 2015. Application of a normalized difference impervious index NDII to extract urban impervious surface features based on Landsat TM images. International Journal of Remote Sensing, 36(4), 1055-1069.
Weng, Q. H., Hu, X. F., & Liu, H., 2009. Estimating impervious surfaces using linear spectral mixture analysis with multitemporal aster images. International Journal of Remote Sensing, 30(18), 4807-4830.
Weng, Q., 2012. Remote sensing of impervious surfaces in the urban areas: requirements, methods, and trends. Remote Sensing of Environment, 117(2), 34-49.
Weng, Q., Hu, X. & Lu. D., 2008. Extracting impervious surfaces from medium spatial resolution multispectral and hyperspectral imagery: a comparison. International Journal of Remote Sensing, 29(11), 3209-3232.
White, M. D., & Greer, K. A., 2006. The effects of watershed urbanization on the stream hydrology and riparian vegetation of los penasquitos creek, california. Landscape & Urban Planning, 74(2), 125-138.
Wu, C., & Murray, A. T., 2003. Estimating impervious surface distribution by spectral mixture analysis. Remote Sensing of Environment, 84(4), 493-505.
Wu, C., & Murray, A. T., 2005. A cokriging method for estimating population density in urban areas. Computers Environment & Urban Systems, 29(5), 558-579.
Wu, C., 2004. Normalized spectral mixture analysis for monitoring urban composition using ETM+ imagery. Remote Sensing of Environment, 93(4), 480-492.
Xian, G., Crane, M., & Su, J., 2007. An analysis of urban development and its environmental impact on the Tampa bay watershed. Journal of Environmental Management, 85(85), 965-76.
Yang, F., Matsushita, B., & Fukushima, T., 2010. A pre-screened and normalized multiple endmember spectral mixture analysis for mapping impervious surface area in lake Kasumigaura basin, Japan. Isprs Journal of Photogrammetry & Remote Sensing, 65(5), 479-490.
Yang, J., & He, Y., 2017. Automated mapping of impervious surfaces in urban and suburban areas: linear spectral unmixing of high spatial resolution imagery. International Journal of Applied Earth Observation & Geoinformation, 54, 53-64.
Yang, L., Huang, C., Homer, C. G., Wylie, B. K., & Coan, M. J., 2003. An approach for mapping large-area impervious surfaces: synergistic use of landsat-7 ETM+ and high spatial resolution imagery. Canadian Journal of Remote Sensing, 29(2), 230-240.

Yang, S., & Lunetta, R. S., 2011. Sub-pixel mapping of tree canopy, impervious surfaces, and cropland in the laurentian great lakes basin using MODIS time-series data. IEEE Journal of Selected Topics in Applied Earth Observations & Remote Sensing, 4(2), 336-347.

Yang, X., & Liu, Z., 2005. Use of satellite-derived landscape imperviousness index to characterize urban spatial growth. Computers Environment & Urban Systems, 29(5), 524-540.

Yuan, F., & Bauer, M. E., 2007. Comparison of impervious surface area and normalized difference vegetation index as indicators of surface urban heat island effects in Landsat imagery. Remote Sensing of Environment, 106(3), 375-386.

Zhang, H., Lin, H., Li, Y., Zhang, Y., & Fang, C., 2016. Mapping urban impervious surface with dual-polarimetric SAR data: an improved method. Landscape & Urban Planning, 151, 55-63.

Zhang, J., He, C., Zhou, Y., Zhu, S., & Shuai, G., 2014. Prior-knowledge-based spectral mixture analysis for impervious surface mapping. International Journal of Applied Earth Observation & Geoinformation, 28(5), 201-210.

Zhang, L. X., Wang, J., Wang, X., & Zhao, J. P., 2007. Competency model of top managers of state-owned enterprise in china's northeastern old industrial base. Journal of Northeastern University, 28(4), 600-604.

Zhang, Y., Zhang, H., & Lin, H., 2014. Improving the impervious surface estimation with combined use of optical and SAR remote sensing images. Remote Sensing of Environment, 141(2), 155-167.

Zhou, Y., & Wang, Y. Q., 2008. Extraction of impervious surface areas from high spatial resolution imagery by multiple agent segmentation and classification. Photogrammetric Engineering & Remote Sensing, 74(7), 857-868.